IOP Publishing Journal of Physics: Condensed Matter
J. Phys.: Condens. Matter **31** (2019) 145601 (5pp) https://doi.org/10.1088/1361-648X/aaffae

Pressure tuning of iron-based superconductor $Ca_{10}(Pt_3As_8)((Fe_{0.95}Pt_{0.05})_2As_2)_5$

X Yin[1,2], C Zhang[3,4,5], G Mu[3,4], T Hu[3,4], M Zhang[2] and H Xiao[1]

[1] Center for High Pressure Science and Technology Advanced Research, Beijing 100094, People's Republic of China
[2] School of Physics and Electronic Technology, Liaoning Normal University, Dalian 116029, People's Republic of China
[3] State Key Laboratory of Functional Materials for Informatics, Shanghai Institute of Microsystem and Information Technology, Chinese Academy of Sciences, 865 Changning Road, Shanghai 200050, People's Republic of China
[4] CAS Center for Excellence in Superconducting Electronics (CENSE), Shanghai 200050, People's Republic of China
[5] University of Chinese Academy of Science, Beijing 100049, People's Republic of China

E-mail: m.zhang@live.com and hong.xiao@hpstar.ac.cn

Received 15 November 2018, revised 4 January 2019
Accepted for publication 17 January 2019
Published 8 February 2019

Abstract

Systematic high pressure transport measurements were performed on underdoped $Ca_{10}(Pt_3As_8)((Fe_{0.95}Pt_{0.05})_2As_2)_5$ single crystal sample. At ambient pressure, the sample shows a metallic behavior at high temperatures and then increases with further decreasing temperature. The resistivity dip, which is associated with metal to semiconductor transition is monotonically suppressed by increasing pressure. In contrast, the superconducting transition temperature T_c first increases with pressure and then decreases with further increasing pressure. Magnetization measurements, which gives the bulk T_c, show the same trend as the one obtained from resistivity measurements. An upward curvature is observed in the temperature dependence of the upper critical field $H_{c2}(T)$, which suggests the multiband nature of the superconductivity. The constructed temperature–pressure ($T-P$) phase diagram is very similar to the reported temperature-doping ($T-x$) phase diagram, suggesting the similar role played by pressure and chemical doping.

Keywords: iron-based superconductor, pressure, phase diagram

(Some figures may appear in colour only in the online journal)

1. Introduction

$Ca_{10}(Pt_nAs_8)((Fe_{1-x}Pt_x)_2As_2)_5$ with $n = 3$ and 4 is a new family of iron-based superconductor [1]. The $n = 3$ (10-3-8) compound is of particular interest because the parent compound is of semiconductor nature which is unusual in iron-based superconductors. In addition, the stoichiometric compound $Ca_{10}(Pt_3As_8)(Fe_2As_2)_5$ is nonsuperconducting and shows no anomaly in the magnetic susceptibility [2]. Nuclear magnetic resonance measurements, however, reveal an antiferromagnetic ground state [3]. Two kinks were found in the derivative of the electrical resistivity around 100 K support the existence of decoupled structural and magnetic phase transitions [4]. The recent combined high resolution high energy x-ray diffraction and inelastic neutron scattering measurements reveal a separate structural ($T_s = 110(2)$ K) and magnetic ($T_N = 96(2)$ K) transition on the same single crystal [5]. A suppression of the spin-lattice relaxation rate observed by nuclear magnetic resonance measurements mark the onset of a pseudogap at 45 K in $Ca_{10}(Pt_3As_8)((Fe_{1-x}Pt_x)_2As_2)_5$ ($T_c = 13$ K) which could be associated with preformed Cooper pairs [6]. This resembles the high temperature cuprate superconductors where nematic

order is observed in the pseudogap regime [7, 8]. Notably, the existence of electronic nematic state is well established in iron-based superconductors [9–12].

$Ca_{10}(Pt_3As_8)(Fe_2As_2)_5$ becomes superconducting by chemical doping, for example, platinum substitution on the Fe site [2], and lanthanum substitution on the Ca site [4]. Multiple superconducting gaps were revealed by muon-spin relaxation [6] and also penetration depth [13] measurements. Superconductivity can also be induced by pressure tuning of the undoped compound and it is found that pressure tuning and chemical doping play similar role in the moderate pressure and doping range but are different at higher pressure and heavy doping regime [14]. One distinguished feature of this material is that there is no overlap between the antiferromagnetic and superconducting phases [14], which is different from the 122 family of iron-based superconductors. This provide a unique opportunity to study superconductivity without the complication due to coexisting phase.

Notably, the semiconductor behavior in $Ca_{10}(Pt_3As_8)((Fe_{1-x}Pt_x)_2As_2)_5$ exists not only in the undoped compound but also survives across the temperature-doping ($T - x$) phase diagram [2]. However, it remains an open question regarding the relationship between the semiconductor behavior, pseudogap and superconductivity. Here, we tune one underdoped sample of $Ca_{10}(Pt_3As_8)((Fe_{0.95}Pt_{0.05})_2As_2)_5$ by applied pressure and study systematically the evolution of both the normal state and superconducting states. This particular sample is chosen since it is close to the optimal doping and no antiferromagnetism is present in the system. We summarized the pressure dependence of the crossover temperature T_{dip} from metallic to semiconductor-like behavior, and also the superconducting transition temperature T_c. The T_{dip} is monotonically decreasing with increasing pressure, while the T_c forms a dome shape, suggesting different origin of the crossover behavior and superconductivity.

2. Experimental details

High quality single crystals of $Ca_{10}(Pt_3As_8)((Fe_{0.95}Pt_{0.05})_2As_2)_5$ were synthesized using a self-flux method [2]. The sample for which the data is shown in this paper has a thickness of 14 μm. Pressure was applied at room temperature using diamond anvil cells (DAC) made of CuBe alloy, with the diamond anvil culet of 800 μm in diameter for electrical resistivity measurements and 500 μm in diameter for magnetization measurements. Electrical resistivity measurements were performed using a Quantum Design physical property measurement system. The Van der Pauw method [15] was used to measure the electrical resistivity and Hall coefficient simultaneously. To determine the bulk superconducting transition temperature, we performed magnetic measurements in a superconducting quantum interference device (SQUID magnetometer). In both cases, Daphne oil 7373 was used as a pressure-transmitting medium, and pressure was calibrated using the ruby fluorescence shift at room temperature.

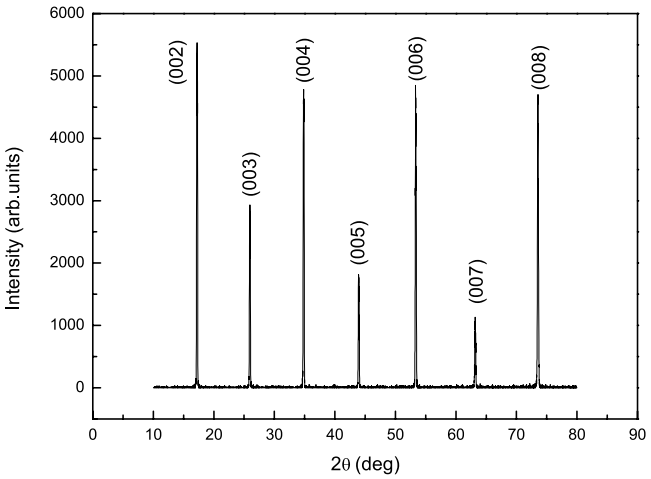

Figure 1. Single crystal x-ray diffraction pattern of $Ca_{10}(Pt_3As_8)((Fe_{0.95}Pt_{0.05})_2As_2)_5$.

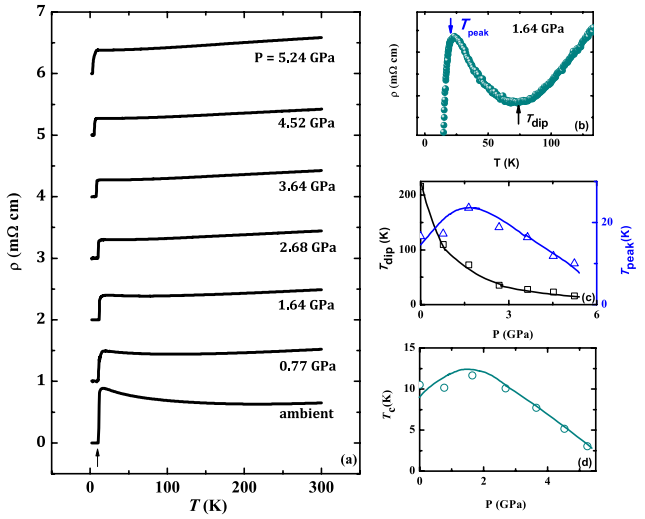

Figure 2. (a) The resistivity versus temperature curves of $Ca_{10}(Pt_3As_8)((Fe_{0.95}Pt_{0.05})_2As_2)_5$ under different pressures, $P = 0, 0.77, 1.64, 2.68, 3.64, 4.52$, and 5.24 GPa. The resistivity were vertically shifted for clarity. (b) The enlarged R versus T curve for $P = 1.64$ GPa to show T_{dip} and T_{peak}. (c) The pressure dependence of T_{dip} and T_{peak}. (d) The superconducting transition temperature T_{c0} versus pressure P.

3. Results and discussion

Figure 1 shows the single-crystal x-ray diffraction pattern of the $Ca_{10}(Pt_3As_8)((Fe_{0.95}Pt_{0.05})_2As_2)_5$ sample. Note that only $(0\,0\,l)$ reflection peaks are observed, which suggest that the single crystal is in perfect $(0\,0\,l)$ orientation.

Figure 2(a) shows the temperature (T) dependent resistivity (ρ) curves measured under applied pressures, $P = 0, 0.77, 1.64, 2.68, 3.64, 4.52$, and 5.24 GPa. The data are shifted vertically for clarity. Note that a different sample is used for the ambient pressure measurements. The resistivity is metallic at higher temperature, reaching a minimum at T_{dip} and then increasing with further decreasing temperature. The low temperature upturn resembles the low pressure data of CaFeAsF parent compound [16] and also doped 1111 system

[17–20]. The upturn becomes less pronounced with increasing pressure, which is similar to the effect of Pt doping [2].

Figure 2(b) shows the enlarged plot of the resistivity data ($P = 1.64$ GPa) in the low temperature regime. The dip and the peak in the resistivity can be clearly observed at $T = 72.7$ K and 23.5 K, respectively. The corresponding superconducting transition temperature is $T_{c0} = 11.6$ K, defined as the temperature for the appearance of zero resistivity. The pressure dependence of T_{dip} and T_{peak} are summarized in figure 2(c). It is found that T_{dip} decreases monotonically with increasing pressure. This tendency is same with the change of T_{dip} with doping [2]. Figure 2(d) plots the pressure dependence of the superconducting transition temperature T_{c0}, which increases slightly and then decreases with increasing pressure, forming a dome shape.

Note that T_{peak} is much higher than T_{c0}. The difference is the largest for $P = 1.64$ GPa, where the difference is as large as 11.9 K. Note that the onset of a pseudogap is reported to be at $T^* = 45$ K in a $Ca_{10}(Pt_3As_8)((Fe_{1-x}Pt_x)_2As_2)_5$ sample with $x = 0.06$ and $T_c = 13$ K, which is likely associated with the emergence of preformed Cooper pairs [6]. Temperature dependent torque data on optimally doped sample [21] show that τ_0 deviate from high temperature T linear behavior at temperature even higher than T^* reported by the nuclear magnetic resonance measurements [6]. Hence, the T_{peak} could be a result of competition of the semiconductor behavior and the superconducting fluctuations in the normal state. In addition, it is found that T_{peak} shows a nonmonotonic pressure dependence and follows well the tendency of T_{c0}.

We made further study on the superconducting state of $Ca_{10}(Pt_3As_8)((Fe_{0.95}Pt_{0.05})_2As_2)_5$ by measuring the superconducting transition in different applied magnetic field. Figures 3(a)–(c) shows the $\rho-T$ curves with $H = 0, 1, 3, 5, 7, 9$ T along c axis at selected pressures, $P = 1.64, 2.68$ and 4.52 GPa. The superconducting transition temperature is gradually suppressed with magnetic field. With increasing pressure, the superconducting transition width becomes broadened. For $P = 4.52$ GPa at higher magnetic fields, the superconducting transition is not complete down to the lowest measured temperature of $T = 2$ K.

Figure 3(d) plots the upper critical field H_{c2} versus temperature T for selected pressures. The superconducting transition temperature T_c is defined as the temperature at which the resistivity goes to zero. It is found that with increasing pressure, the H_{c2} is monotonically suppressed. There is a clear upward curvature in $H_{c2}(T)$, which can not be explained by the one-gap Werthamer–Helfand–Hohenberg theory and may be attributed to the effect of a two-gap scenario. And indeed, muon-spin relaxation (μSR) measurements revealed the presence of two superconducting gaps, with $\Delta_1 = 2.13 \pm 0.13$ meV and $\Delta_2 = 0.33 \pm 0.31$ meV [6]. This suggests the multiband nature of superconductivity in $Ca_{10}(Pt_3As_8)((Fe_{0.95}Pt_{0.05})_2As_2)_5$ under pressure. The upward curvature of $H_{c2}(T)$ is also observed in the 10-4-8 phase [22] and CaFeAsF [16]. The $H_{c2}(T)$ data can be described within the entire temperature range by the empirical equation $H_{c2}(T) = H_{c2}(0)(1 - T/T_c)^n$ [16, 23], which gives

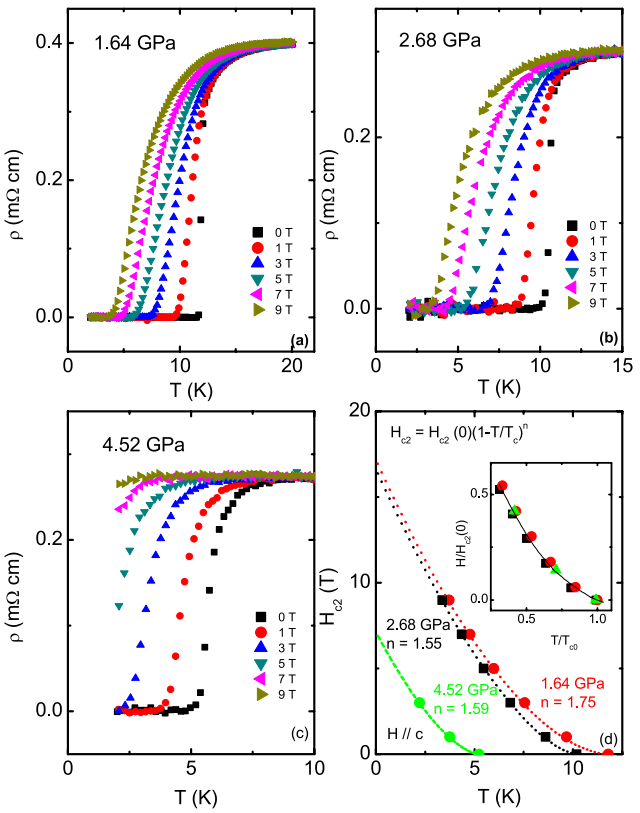

Figure 3. (a)–(c) Show typical low-temperature-dependent resistivity curves for $Ca_{10}(Pt_3As_8)((Fe_{0.95}Pt_{0.05})_2As_2)_5$ with $H = 0, 1, 3, 5, 7$ and 9 T parallel to the c axis at $P = 1.64, 2.68$ and 4.52 GPa, respectively. (d) The representative temperature T dependent upper critical field H_{c2} curves. The dashed lines are fitting curves by $H_{c2}(T) = H_{c2}(0)(1 - T/T_c)^n$. Inset shows the reduced magnetic field H/H_{c2} versus the reduced temperature T/T_{c0}.

a $H_{c2}(0)$ of 14.1–17.2 T and the exponent n ranges from 1.55–1.75 in the pressure range between 1.64–4.52 GPa. The inset shows the reduced magnetic field $H/H_{c2}(0)$ versus the reduced temperature T/T_{c0} curves. It is found that the data for different pressures overlap.

To determine the bulk superconducting transition temperature we performed zero-field-cooled magnetization measurements under different pressures namely, $P = 0.6, 0.94, 1.2, 1.9, 2.5, 3.2, 3.8$, and 4.4 GPa as shown in figure 4(a). Since the sample used in the pressure cell is too small to measure its mass, here we show the magnetization data in emu. Figure 4(b) shows the pressure dependence of the superconducting transition temperature obtained from magnetization data. It is found that $T_{c,m}$ increases first, reaches a maximum and then decreases fast with P, consistent with the overall tendency of T_c determined from electrical resistivity data.

Next, we study Hall resistivity ρ_{xy} which is measured simultaneously with resistivity by sweeping the magnetic field from −9 to 9 T. The electric current is applied along the ab plane and the magnetic field along the c axis. Figure 5(a) shows the magnetic field H dependence of the Hall resistivity ρ_{xy} at $T = 20$ K. For clarity, we show only data at $P = 1.64, 3.64$ and 5.24 GPa. It is found that ρ_{xy} varies linearly with H at all

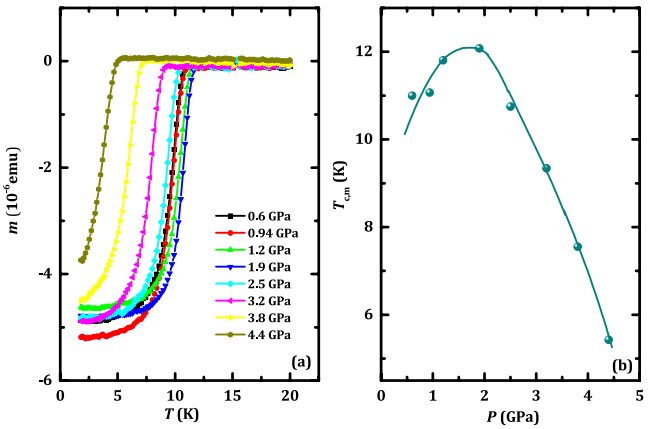

Figure 4. Temperature dependence of magnetization measured at $P = 0.6, 0.94, 1.2, 1.9, 2.5, 3.2, 3.8$ and 4.4 GPa in an applied magnetic field of 10 Oe. (b) Pressure dependence of the superconducting transition temperature $T_{c,m}$ determined from magnetization measurements.

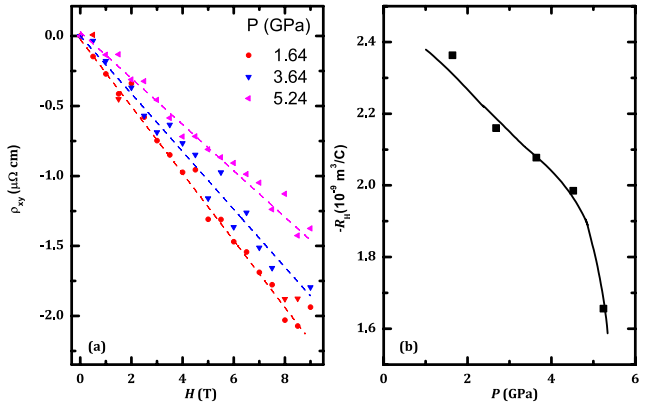

Figure 5. (a) Magnetic field H dependence of Hall resistivity ρ_{xy} at pressure $P = 1.64, 3.64$, and 5.24 GPa. The dashed lines are linear fitting curves. (b) Pressure dependence of Hall coefficient R_H at $T = 20$ K. The solid line is a guide to the eye.

pressures, which suggests that only one type of charge carrier dominates transport at this particular temperature [24, 25]. The calculated Hall coefficient R_H is shown in figure 5(b). The value of R_H is comparable with a previous report on $Ca_{10}(Pt_3As_8)((Fe_{1-x}Pt_x)_2As_2)_5$ [2], and other iron-based superconductors, $(Ba_{1-x}La_x)Fe_2As_2$ [26] and $NaFe_{1-x}Rh_xAs$ [27]. Note that R_H decreases with increasing pressure and this tendency is similar to the pressure dependence of R_H obtained for the undoped parent compound [14].

Figure 6 shows the summarized temperature versus pressure $T-P$ phase diagram. The crossover temperature T_{dip} from metallic to semiconductor behavior is monotonically suppressed with increasing pressure. The superconducting transition temperature T_c increases initially and then decreases with increasing pressure. The dome shape of T_c with P is similar to that of 122 family of iron-based superconductor [28–31], but different from 1111 family, for example, CaFeAsF, where T_c is monotonically suppressed with increasing pressure [16, 32]. The resistivity maximum T_{peak}, which is a result of competition between semiconductor behavior and superconducting fluctuations above T_c, follows well the tendency of

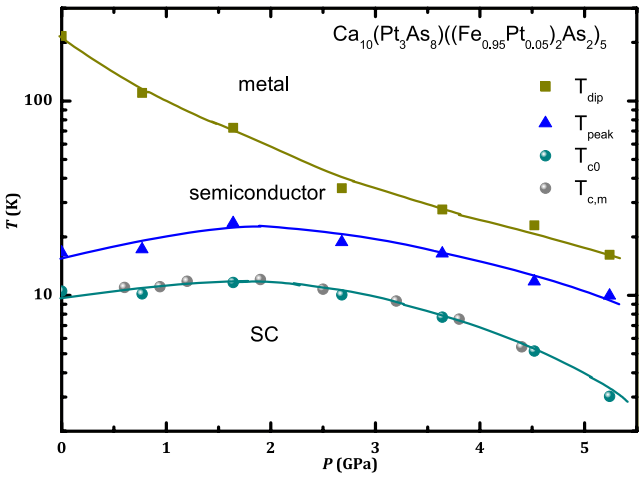

Figure 6. Temperature versus pressure ($T-P$) phase diagram of $Ca_{10}(Pt_3As_8)((Fe_{0.95}Pt_{0.05})_2As_2)_5$. T_{dip} is the resistivity minimum which corresponds to the crossover temperature from metallic and semiconductor-like behavior. T_{peak} represents the temperature of the resistivity maximum before entering the superconducting state. The superconducting transition temperature T_{c0} and $T_{c,m}$ are determined from resistivity and magnetization measurement, respectively.

the pressure dependence of T_c. The $T-P$ phase diagram show great resemblance to the reported $T-x$ phase diagram [2], suggesting the similar role of pressure and chemical doping in superconducting $Ca_{10}(Pt_3As_8)((Fe_{1-x}Pt_x)_2As_2)_5$ samples.

4. Conclusions

In summary, we have performed resistivity and magnetization measurements under pressure and constructed the temperature-pressure phase diagram of $Ca_{10}(Pt_3As_8)((Fe_{0.095}Pt_{0.05})_2As_2)_5$. With increasing pressure, the crossover temperature from metal to semiconductor behavior decreases, hence the material becomes more metallic. The superconducting transition temperature T_c forms a dome shape. In addition, the T_{peak} follows well the pressure dependence of T_{c0} and could be a result of competition of the semiconductor behavior and the superconducting fluctuations in the normal state. Comparing the obtained $T-P$ phase diagram and the reported $T-x$ phase diagram, we concluded that pressure plays a similar role as chemical doping in the superconducting sample of $Ca_{10}(Pt_3As_8)((Fe_{1-x}Pt_x)_2As_2)_5$.

Acknowledgments

Work at HPSTAR was supported by NSAF, grant No. U1530402. Work at SIMIT was supported by the support of NSFC, grant No. 11574338 and the Youth Innovation Promotion Association of the Chinese Academy of Sciences (grant No. 2015187). M Zhang acknowledges the support from NSFC, grant No. 51101080.

ORCID iDs

H Xiao https://orcid.org/0000-0001-8859-9967

References

[1] Ni N, Allred J M, Chan B C and Cava R J 2011 *Proc. Natl Acad. Sci.* **108** 18201
[2] Xiang Z J, Luo X G, Ying J J, Wang X F, Yan Y J, Wang A F, Cheng P, Ye G J and Chen X H 2012 *Phys. Rev.* B **85** 224527
[3] Zhou T, Koutroulakis G, Lodico J, Ni N, Thompson J D, Cava R J and Brown S E 2013 *J. Phys.: Condens. Matter* **25** 122201
[4] Ni N, Straszheim W E, Williams D J, Tanatar M A, Prozorov R, Bauer E D, Ronning F, Thompson J D and Cava R J 2013 *Phys. Rev.* B **87** 060507
[5] Sapkota A, Tucker G S, Ramazanoglu M, Tian W, Ni N, Cava R J, McQueeney R J, Goldman A I and Kreyssig A 2014 *Phys. Rev.* B **90** 100504
[6] Surmach M A *et al* 2015 *Phys. Rev.* B **91** 104515
[7] Daou R *et al* 2010 *Nature* **463** 519
[8] Ando Y, Komiya S, Segawa K, Ono S and Kurita Y 2004 *Phys. Rev. Lett.* **93** 267001
[9] Lu X, Park J T, Zhang R, Luo H, Nevidomskyy A H, Si Q and Dai P 2014 *Science* **345** 657
[10] Chu J-H, Analytis J G, De Greve K, McMahon P L, Islam Z, Yamamoto Y and Fisher I R 2010 *Science* **329** 824
[11] Kasahara S *et al* 2012 *Nature* **486** 382
[12] Kuo H-H, Chu J-H, Riggs S C, Yu L, McMahon P L, De Greve K, Yamamoto Y, Analytis J G and Fisher I R 2011 *Phys. Rev.* B **84** 054540
[13] Watson M D *et al* 2014 *Phys. Rev.* B **89** 205136
[14] Gao P *et al* 2014 *Adv. Mater.* **26** 2346
[15] van der Pauw L J 1959 *Philips Tech. Rev.* **20** 220
[16] Gao B, Ma Y, Mu G and Xiao H 2018 *Phys. Rev.* B **97** 174505
[17] Cao G *et al* 2009 *Phys. Rev.* B **79** 174505
[18] Wang C *et al* 2009 *Phys. Rev.* B **79** 054521
[19] Xiao H, Gao B, Ma Y H, Li X J, Mu G and Hu T 2016 *J. Phys.: Condens. Matter* **28** 325701
[20] Ma Y, Hu K, Ji Q, Gao B, Zhang H, Mu G, Huang F and Xie X 2016 *J. Cryst. Growth* **451** 161
[21] Yang R, Dai Y, Yu J, Sui Q, Ren Z, Hwang J, Xiao H, Qiu X, Run Yang, Dai Y and Homes C C 2018 unpublished
[22] Yuan F F, Sun Y, Zhou W, Zhou X, Ding Q P, Iida K, Hhne R, Schultz L, Tamegai T and Shi Z X 2015 *Appl. Phys. Lett.* **107** 012602
[23] Pan X-C *et al* 2015 *Nat. Commun.* **6** 7805
[24] Xu G, Wang W, Zhang X, Du Y, Liu E, Wang S, Wu G, Liu Z and Zhang X X 2014 *Sci. Rep.* **4** 5709
[25] Zhang M, Zhang C, Yu Y, Zhang L, Qu Z, Ling L, Xi C, Tan S and Zhang Y 2010 *New J. Phys.* **12** 083050
[26] Katase T, Sato H, Hiramatsu H, Kamiya T and Hosono H 2013 *Phys. Rev.* B **88** 140503
[27] Steckel F, Caglieris F, Beck R, Roslova M, Bombor D, Morozov I, Wurmehl S, Büchner B and Hess C 2016 *Phys. Rev.* B **94** 184514
[28] Liu W *et al* 2018 *Phys. Rev.* B **97** 144515
[29] Colombier E, Torikachvili M S, Ni N, Thaler A, Bud'ko S L and Canfield P C 2010 *Supercond. Sci. Technol.* **23** 054003
[30] Hassinger E *et al* 2012 *Phys. Rev.* B **86** 140502
[31] Li B, Lu P, Liu J, Sun J, Li S, Zhu X and Wen H-H 2016 *Sci. Rep.* **6** 24479
[32] Okada H, Takahashi H, Matsuishi S, Hirano M, Hosono H, Matsubayashi K, Uwatoko Y and Takahashi H 2010 *Phys. Rev.* B **81** 054507